

NIR-II light-response porphyrin-heptazine-based conjugated organic polymers for highly efficient photooxidation

Lin-Fang Yang, Cheng-Cheng Zhang, Yi-Zhou Zhu,* and Jian-Yu Zheng*

State Key Laboratory and Institute of Elemento-Organic Chemistry, College of
Chemistry, Nankai University, Tianjin 300071, China. E-mail:
zhuyizhou@nankai.edu.cn (Yi-Zhou Zhu); jyzheng@nankai.edu.cn (Jian-Yu Zheng).

Tel: +86-22-2350 5572; Fax: +86-22-2350 5572.

Contents

1.	Experimental Section	1
2.	Characterization.....	6
3.	Structural optimization.....	8
4.	Photooxidation of 1,4-DHP (10^{-4} M).....	9
5.	NMR spectra of the product.	12
6.	Photooxidation of 1,4-DHP (10^{-3} M).....	13
7.	ICP results of MTPP-Cys.	15
8.	Cycling stability of H_2 TPP-Cy.....	15
9.	Summary of recently reported literatures for photooxidation of 1,4-DHP.....	17
10.	References	18

1. Experimental Section

1.1 Reagents

All reagents were used as received unless otherwise noted. 5,10,15,20-Tetraphenylporphyrin (H₂TPP), melamine, cupric (II) acetate monohydrate, nickel (II) acetate tetrahydrate, phosphorus oxychloride, phosphorus pentachloride and aluminum chloride were purchased from Anhui Zesheng Technology Co., Ltd. Dichloromethane (DCM) was dried by distillation with CaH₂.

1.2 Materials Characterization

Solution-state ¹H NMR and ¹³C NMR spectroscopies were recorded on a 400 MHz spectrometer (Bruker Ascend 400 Spectrometer) with tetramethylsilane as internal standard. Solid-state ¹³C cross polarization magic angle spinning NMR spectroscopies (CP-MAS NMR) were performed by VANCE NEO 400 spectrometer, equipped with a 9.4 T magnet. Fourier transform infrared spectra (FT-IR) were recorded on a Thermofisher Scientific Nicolet iS50 spectrometer between 4000-400 cm⁻¹. Powder X-ray diffraction (PXRD) patterns were obtained on a Japan Rigaku SmartLab diffractometer. X-ray photoelectron spectroscopies (XPS) were performed on an Axis Ultra DLD spectrometer, equipped with a prereduction chamber. Scanning electron microscopies (SEM) were measured on a FEI Apreo S LoVac microscope. The UV-Vis absorption spectra were recorded on a UV-Vis DRS PE lambda 750 spectrophotometer, equipped with an integrating sphere assembly and BaSO₄ was used as reflectance sample. Metal contents were measured by inductively coupled plasma optical emission spectrometer (ICP-OES, SpectroBlue, Germany). Nitrogen adsorption-desorption isotherms were obtained on a nitrogen adsorption apparatus (Surface Area and Pore Analyzer Micromeritics ASAP 2460) with all samples degassed at 373 K for 12 h prior to measurements. Steady-state photoluminescence (PL) spectra were collected by a HITACHI F-4600 spectrofluorometer.

1.3 Theoretical Calculation

Theoretical calculations were carried out using the Gaussian 09 software package.^{1,2} All calculations were performed using the density functional theory (DFT) method. The geometries were optimized at the B3LYP-D3/6-31+G(d) level, and the energies were calculated at the same level.

1.4 Photocatalytic Oxidation

Photocatalytic oxidation reaction was performed according to the reported literatures with some modification.³⁻⁶ Experiments were carried out at room temperature under air atmosphere, in a 50 mL quartz photoreactor with irradiation by a 300 W xenon lamp (30 mW cm⁻²). The ethanol/water (v/v = 1/1) solution of 1,4-DHP (20 mL, 1 × 10⁻⁴ M or 1 × 10⁻³ M) and 20 mg photocatalyst was added to the photoreactor and then irradiated at $\lambda > 420$ nm. The reaction process was monitored by the spectral change of either the decreased absorption intensity of 1,4-DHP at 374 nm or the increased absorption intensity of the oxidative product at 280 nm.

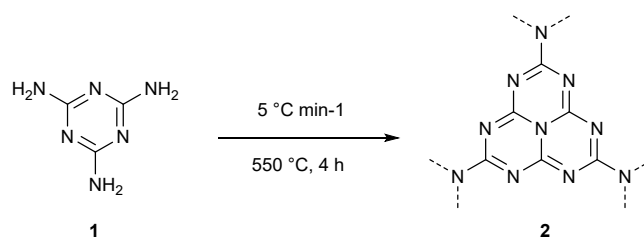
1.5 Electrochemical Experiments

Photocurrent response experiments and electrochemical impedance spectroscopy (EIS) were performed on a Zennium electrochemical workstation (ZAHNER, Germany) with a standard three-electrode cell using Ag/AgCl electrode as the reference electrode, a Pt wire as the counter electrode, sample deposited indium tin oxide (ITO) glass plate as the working electrode, and 0.1 M Na₂SO₄ aqueous solution as the electrolyte solution. The working electrode was manufactured as follows: 2.5 mg catalyst was dispersed in a mixture solution of 225 μ L ethanol, 250 μ L H₂O and 25 μ L Nafion, and sonicated for 30 min. Then, the suspension was transferred onto a 1 cm × 2 cm ITO conductive glass and dried at 60°C. The exposure area of the catalyst is 1 cm². The photocurrent density measurements were performed at a 0.05 V bias potential under visible light ($\lambda > 420$ nm, 300 W Xenon light). The EIS datas were obtained using a frequency ranged from 10⁶ Hz to 10⁻¹ Hz with the open circuit potential at 0.01 V.

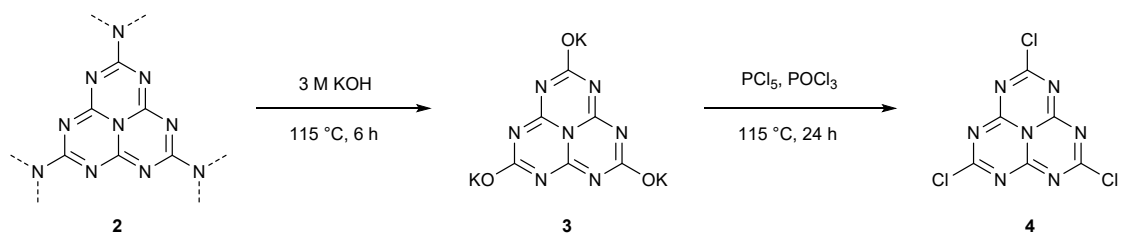
1.6 Electron Paramagnetic Resonance (EPR) Measurements

Spin trapping-EPR and unpaired electrons-EPR measurements were recorded using a Bruker EPR spectrometer operating at the X-band frequency (9.85 GHz). For Spin trapping-EPR measurements, 5,5-dimethyl-1-pyrroline *N*-oxide (DMPO) were used to detect superoxide anion radical ($\text{O}_2^{\cdot-}$). The detailed measurements were conducted as follows: catalysts (1 mg L^{-1}) were dispersed in a mixed solution of DMPO (20 mmol L^{-1}) and 1,4-DHP (5 mL , $1 \times 10^{-3} \text{ mol L}^{-1}$). Before spin trapping-EPR tests, the mixture was stirred for 30 min under light ($\lambda > 420 \text{ nm}$, 300 W Xenon light) or in darkness and then transported into quartz capillaries. For unpaired electrons-EPR measurements, catalyst ($\sim 5 \text{ mg}$) was injected into quartz capillaries without further treatment.

1.7 Synthetic Procedure

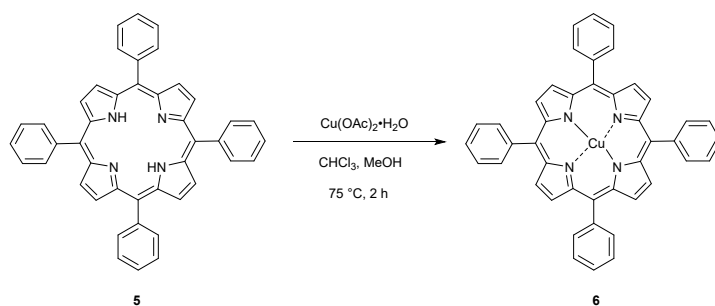


Synthesis of g-C₃N₄ (2).⁷ Melamine (40.0 g, 317.2 mmol) was placed in a ceramic crucible and heated to 550°C at a rate of 5°C min⁻¹ in a muffle furnace and stood for 4 h. After completed, the system was cooled to room temperature at an unrestricted rate and then the solid was ground to obtain compound **2** as a yellow powder.



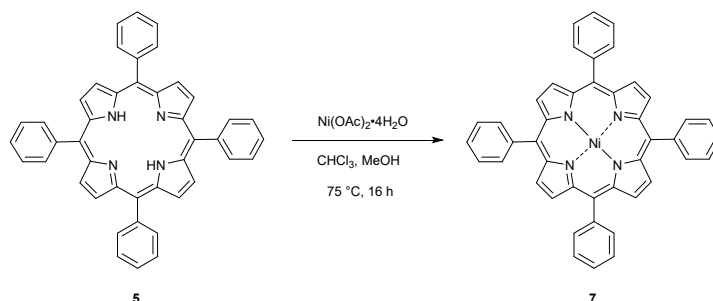
Synthesis of Cymeluric Chloride (4).⁸ Compound **2** (10 g) was dispersed in an aqueous solution of KOH (3 M, 150 mL) and then the mixture was heated at 115 °C for 6 h. The solution was filtered while hot and the filtrate was cooled in an ice-water bath. After that, the precipitated white crystals were collected by filtration and washed with ice ethanol. Finally, the products were dried in a vacuum oven at 80°C for 24 h without further treatment.

Compound **3** (6 g, 17.9 mmol) and PCl₅ (12 g, 57.7 mmol) was dispersed in POCl₃ (120 mL) in argon atmosphere. The mixture was heated at 115°C for 24 h. After completed, the mixture was filtered and the filtrate was removed by rotary evaporator. The residue was further treated by Soxhlet extraction with toluene for 24 h. Then, the solvent was removed by rotary evaporator and the residue dried under vacuum for 6 h, giving the final product **4** as a light-yellow solid (3.5 g, 72%). IR (KBr, cm⁻¹): 1643, 1608, 1502, 1451, 1377, 1302, 1199, 1095, 957, 831, 647, 452. ¹³C NMR (400 MHz, benzene-*d*₆, ppm): δ 175.3 (N-C=N), 155.4 (C-Cl).



Synthesis of Cu(II)-Tetraphenylporphyrin (6, CuTPP).⁹ Compound **5** (760 mg, 1.24 mmol) and Cu(OAc)₂·H₂O (1.361 g, 6.2 mmol) were dissolved in a mixed solution of CHCl₃ and MeOH (300 mL, v/v = 2:1) and then the solution was refluxed at 75°C for 2 h. After completed, the mixture was cooled to room temperature and then poured into water, extracted with chloroform. The organic layer was dried over

Na₂SO₄. After filtered, the solvent was removed by rotary evaporator, giving compound **6** as a red and black solid (793 mg, 95%). FTIR (KBr, cm⁻¹): 3052, 2921, 1597, 1440, 1345, 1070, 1004, 793, 742, 697. MS (MALDI-TOF): m/z calcd for CuC₄₄H₂₈N₄, [M+H]⁺:676.3; found: 677.1.



Synthesis of Ni(II)-Tetraphenylporphyrin (7, NiTPP).¹⁰ Compound **5** (760 mg, 1.24 mmol) and Ni(OAc)₂·4H₂O (622 mg, 3.72 mmol) were dissolved in a mixed solution of CHCl₃ and MeOH (300 mL, v/v = 2:1) and then the solution was refluxed at 75°C for 16 h. When completed, the mixture was cooled to room temperature. After removal of the solvents under reduced pressure, the residue was purified via column chromatography over silica gel (eluent: from PE/DCM = 2:1, v/v to DCM), giving compound **7** as a purple and black solid (640 mg, 77%). ¹H NMR (400 MHz, CDCl₃, ppm): δ 7.68 (d, 12H), 8.02 (d, 8H), 8.74 (s, 8H). The FTIR spectra of NiTPP is similar with CuTPP. MS (MALDI-TOF): m/z calcd for C₄₄H₂₈N₄Ni, [M+H]⁺: 671.4; found: 671.7.

Synthesis of Heptazine-Based Polymers (MTPP-Cys). In general, free-base or metalated tetraphenylporphyrins (0.75 mmol) and Cy (1 mmol) were dissolved in anhydrous DCM (50 mL) in argon atmosphere. The system was kept at 25°C and anhydrous AlCl₃ (14.5 mmol) was added. Then, the mixture was refluxed with 55°C oil-bath for 72 h. After that, the system was cooled to room temperature and then filtered to obtain the crude product, which was washed successively with HCl (1 M), methanol and DCM. Further purification was carried out by Soxhlet extraction with the mixture of methanol and THF for 24 h. Finally, the products were dried in a vacuum oven at 80°C for 24 h.

2. Characterization

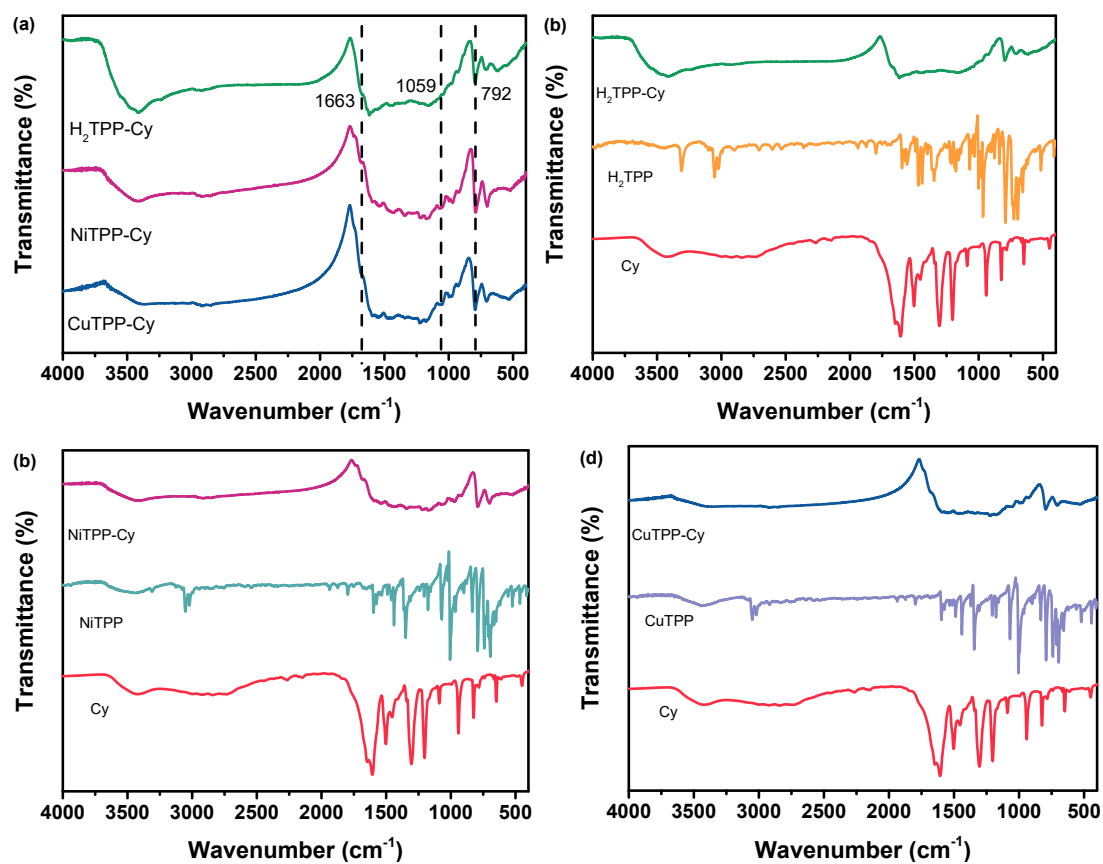


Figure S1. FT-IR spectra. (a) MTPP-Cys; (b) H₂TPP-Cy, (c) NiTPP-Cy, (d) CuTPP-Cy and their corresponding precursors.

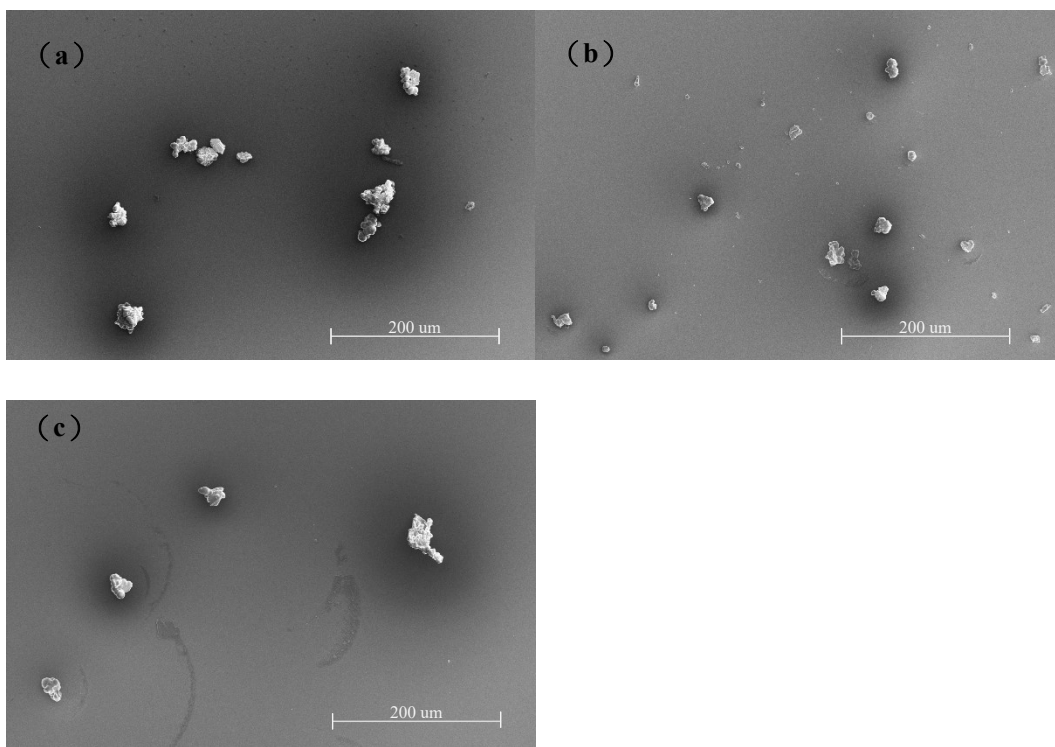


Figure S2. SEM spectra of MTPP-Cys. (a) H₂TPP-Cy; (b) NiTPP-Cy; (c) CuTPP-Cy.

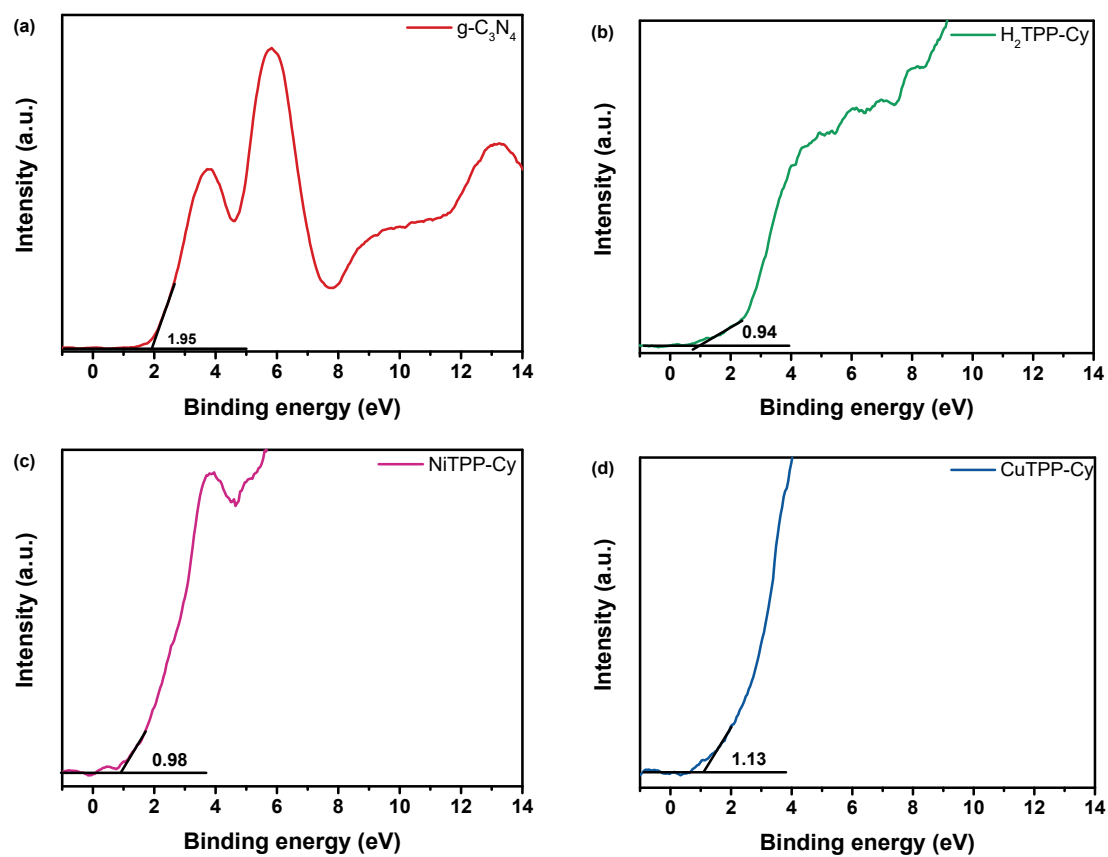


Figure S3. Valence band XPS spectra of $g\text{-C}_3\text{N}_4$ and MTPP-Cys. (a) $g\text{-C}_3\text{N}_4$; (b) H₂TPP-Cy; (c) NiTPP-Cy; (d) CuTPP-Cy.

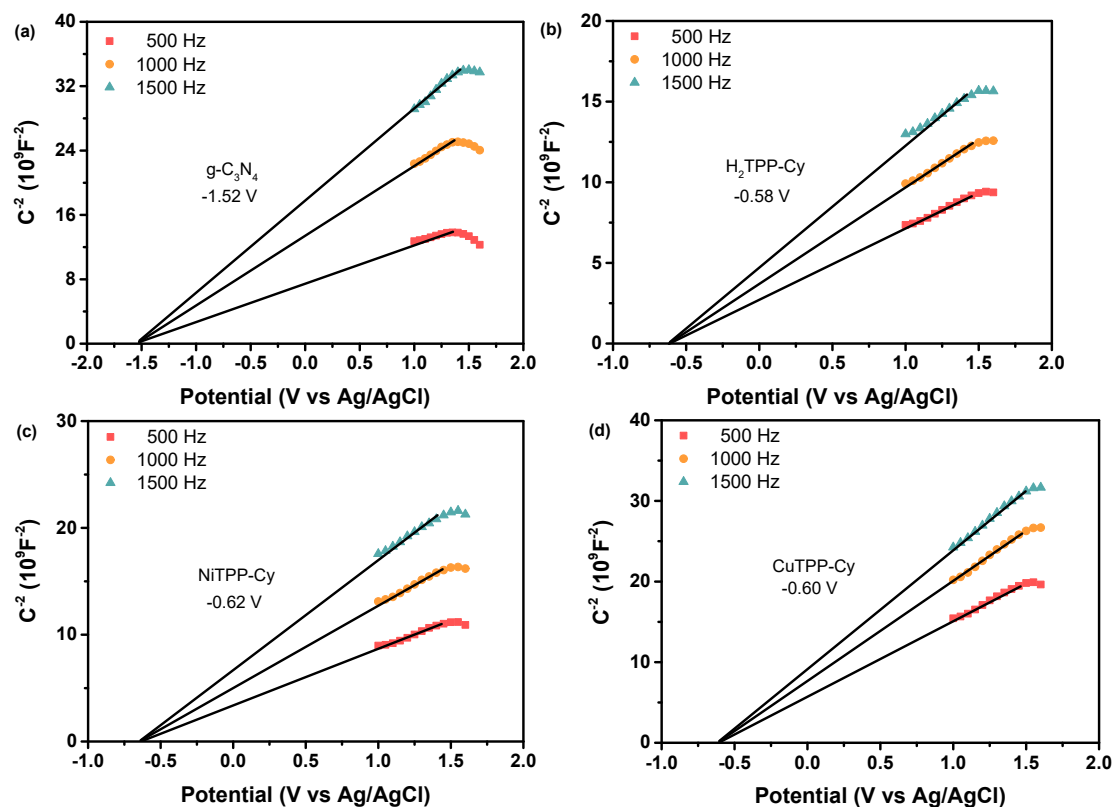


Fig S4. The determined flat-band potential of (a) $g\text{-C}_3\text{N}_4$, (b) $\text{H}_2\text{TPP-Cy}$, (c) NiTPP-Cy , (d) CuTPP-Cy by the Mott-Schottky method.

3. Structural optimization

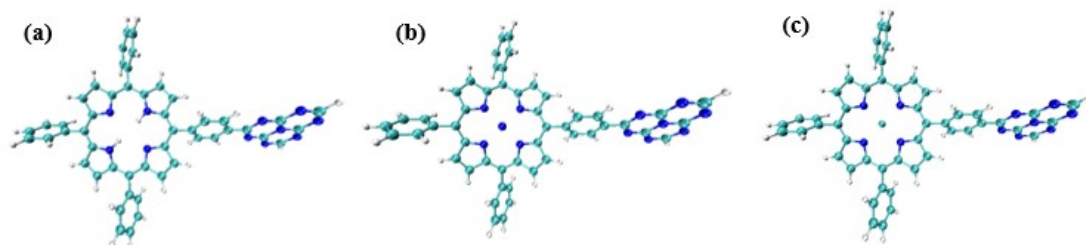


Figure S5. Structural optimization of MTPP-Cys by theoretical calculation. (a) $\text{H}_2\text{TPP-Cy}$; (b) NiTPP-Cy ; (c) CuTPP-Cy .

4. Photooxidation of 1,4-DHP (10^{-4} M).

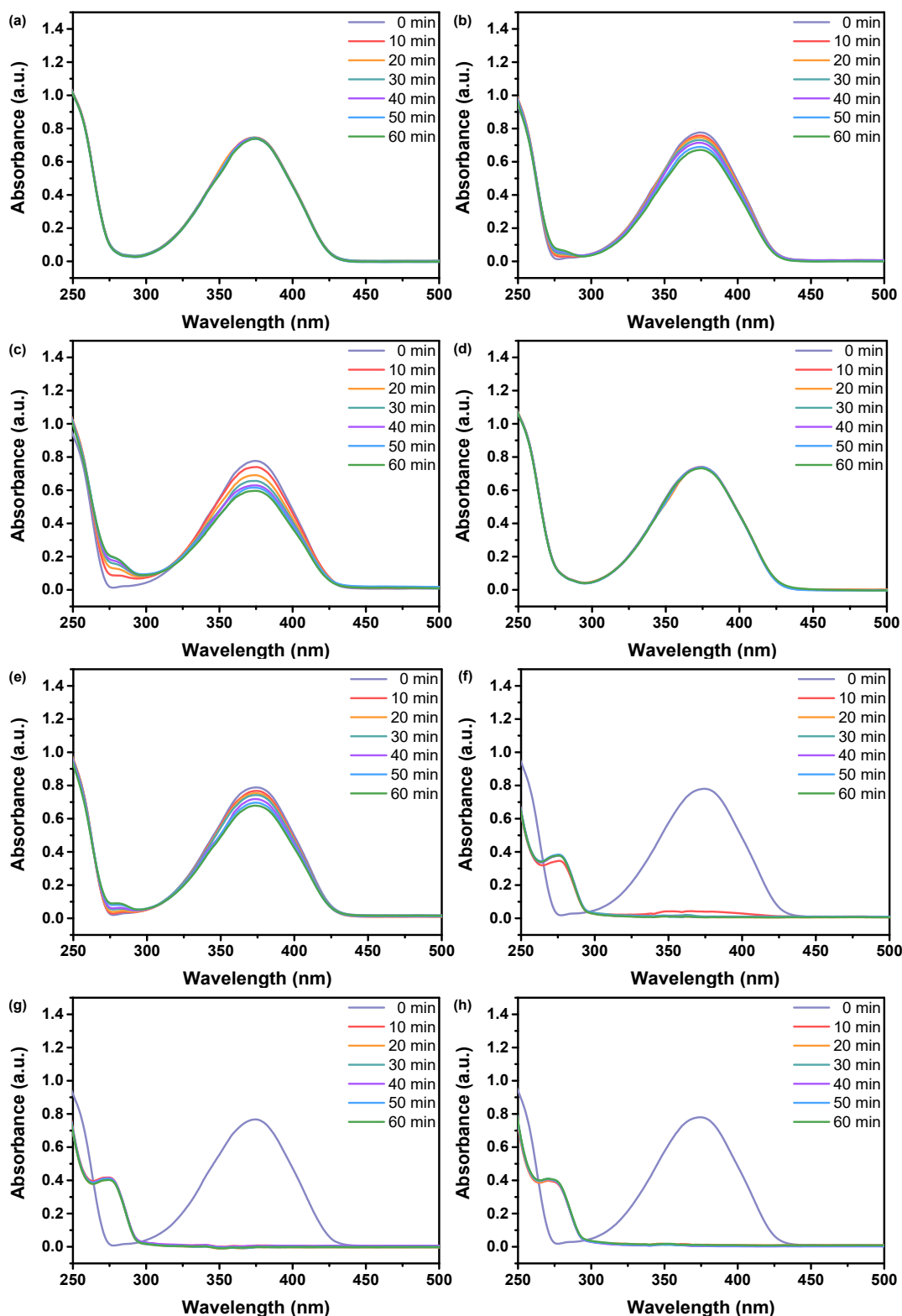


Figure S6. UV-vis absorption spectral change for the photooxidation of 1,4-DHP (10^{-4} M) catalyzed by different catalysts under irradiation with a xenon lamp ($\lambda > 420$ nm). (a) none; (b) $g\text{-C}_3\text{N}_4$; (c) CuTPP; (d) NiTPP; (e) H_2TPP ; (f) CuTPP-Cy; (g) NiTPP-Cy; (h) H_2TPP -Cy.

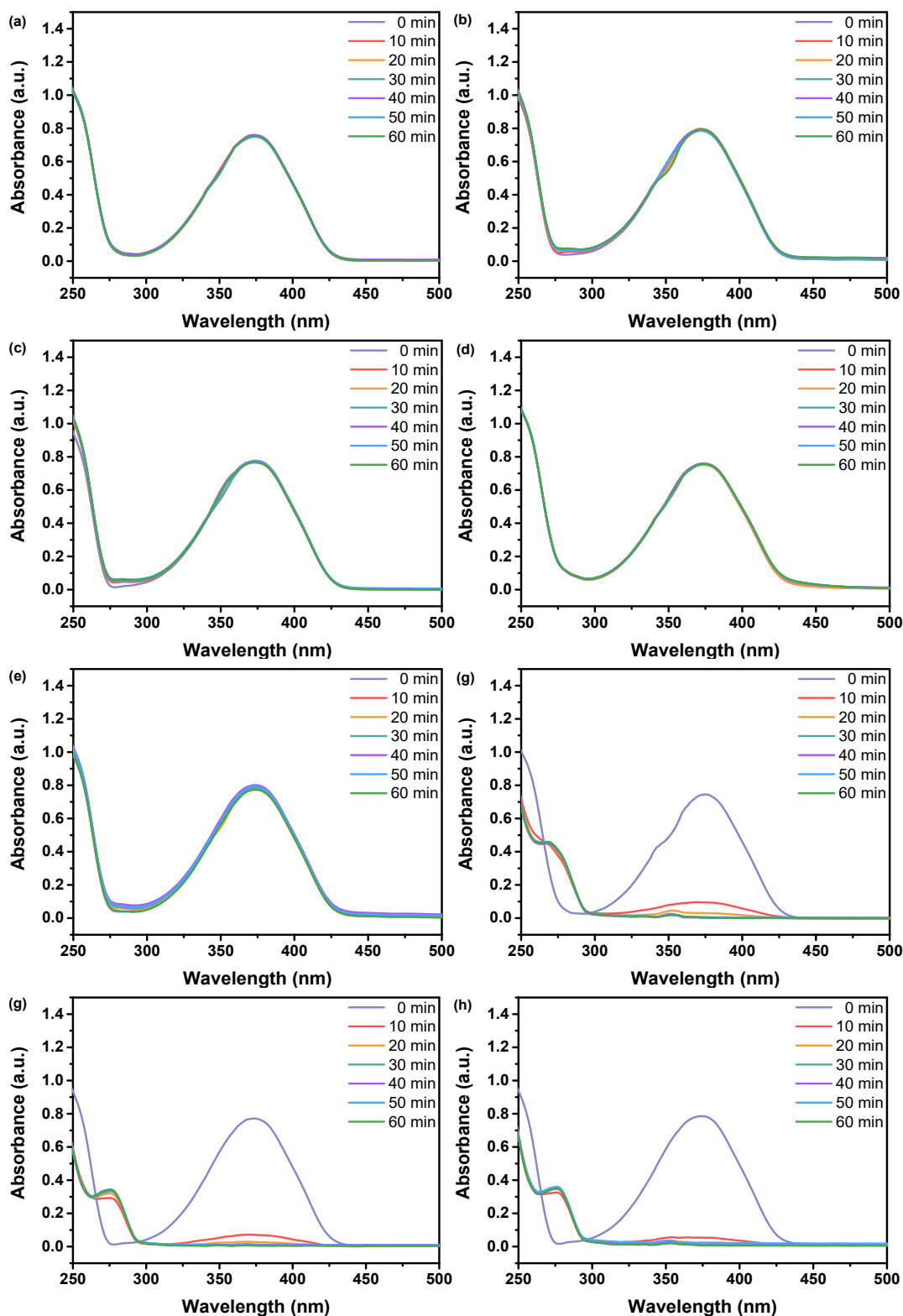
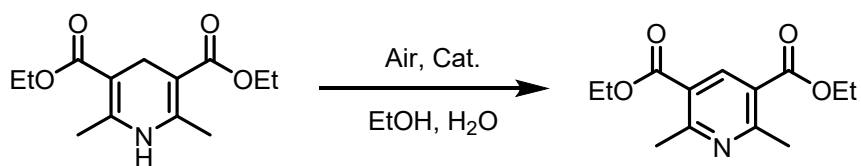


Figure S7. UV-vis absorption spectral change for the photooxidation of 1,4-DHP (10^{-4} M) catalyzed by different catalysts in darkness. (a) none; (b) $g\text{-C}_3\text{N}_4$; (c) CuTPP; (d) NiTPP; (e) H_2TPP ; (f) CuTPP-Cy; (g) NiTPP-Cy; (h) H_2TPP -Cy.

Table S1. Photooxidation of 1,4-DHP (10^{-4} M) catalyzed by different catalysts.

Entries ^a	Catalyst	Conditions ^b	Time/min	Conversion ^c %
1	None	darkness	60	0
2	None	Light	60	0
3	g-C ₃ N ₄	darkness	60	0
4	g-C ₃ N ₄	Light	60	14
5	CuTPP	darkness	60	0
6	CuTPP	Light	60	23
7	NiTPP	darkness	60	0
8	NiTPP	Light	60	0
9	H ₂ TPP	darkness	60	0
10	H ₂ TPP	Light	60	14
11	CuTPP-Cy	darkness	≤30	>99
12	CuTPP-Cy	Light	≤20	>99
13	NiTPP-Cy	darkness	≤30	>99
14	NiTPP-Cy	Light	≤10	>99
15	H ₂ TPP-Cy	darkness	≤20	>99
16	H ₂ TPP-Cy	Light	≤10	>99

^a C_{catalysts} = 1 mg mL⁻¹, V_{solvent} = 20 mL (EtOH and H₂O, v/v = 1:1), C_{1,4-DHP} = 10⁻⁴ M

^b In darkness or under irradiation with a xenon lamp ($\lambda > 420$ nm).

^c Determined by UV-Vis spectroscopy.

5. NMR spectra of the product.

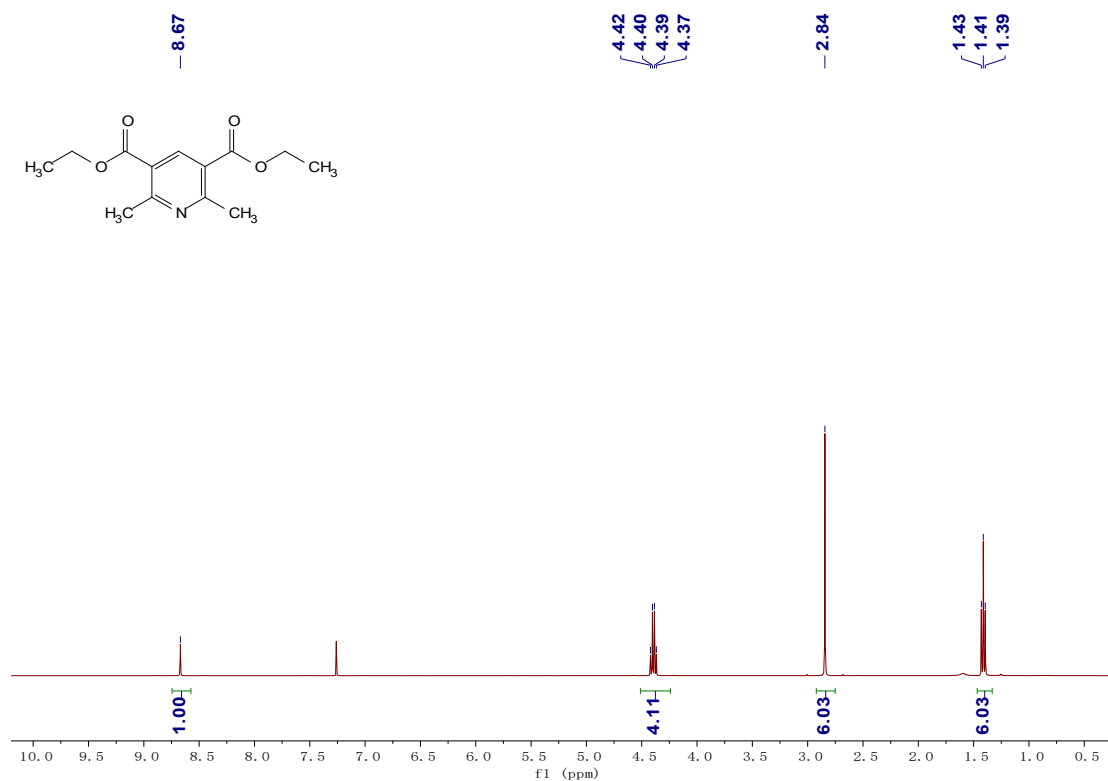


Figure S8. ¹H NMR spectrum of the product.

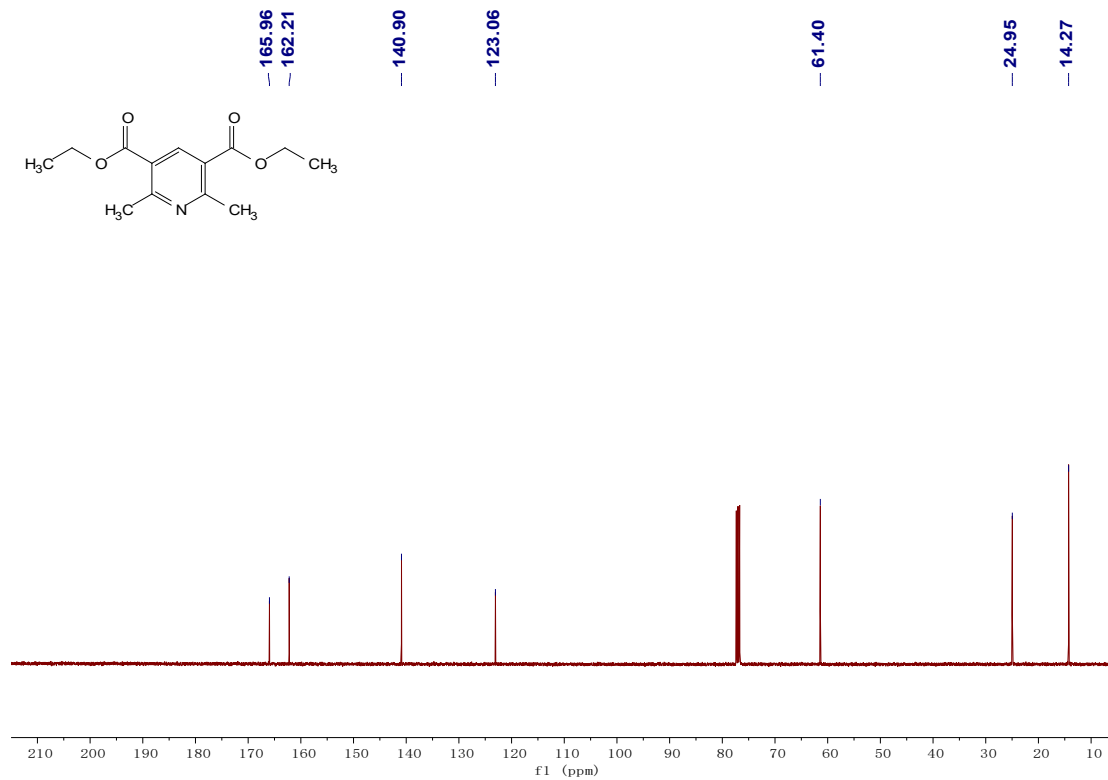


Figure S9. ¹³C NMR spectrum of the product.

6. Photooxidation of 1,4-DHP (10^{-3} M).

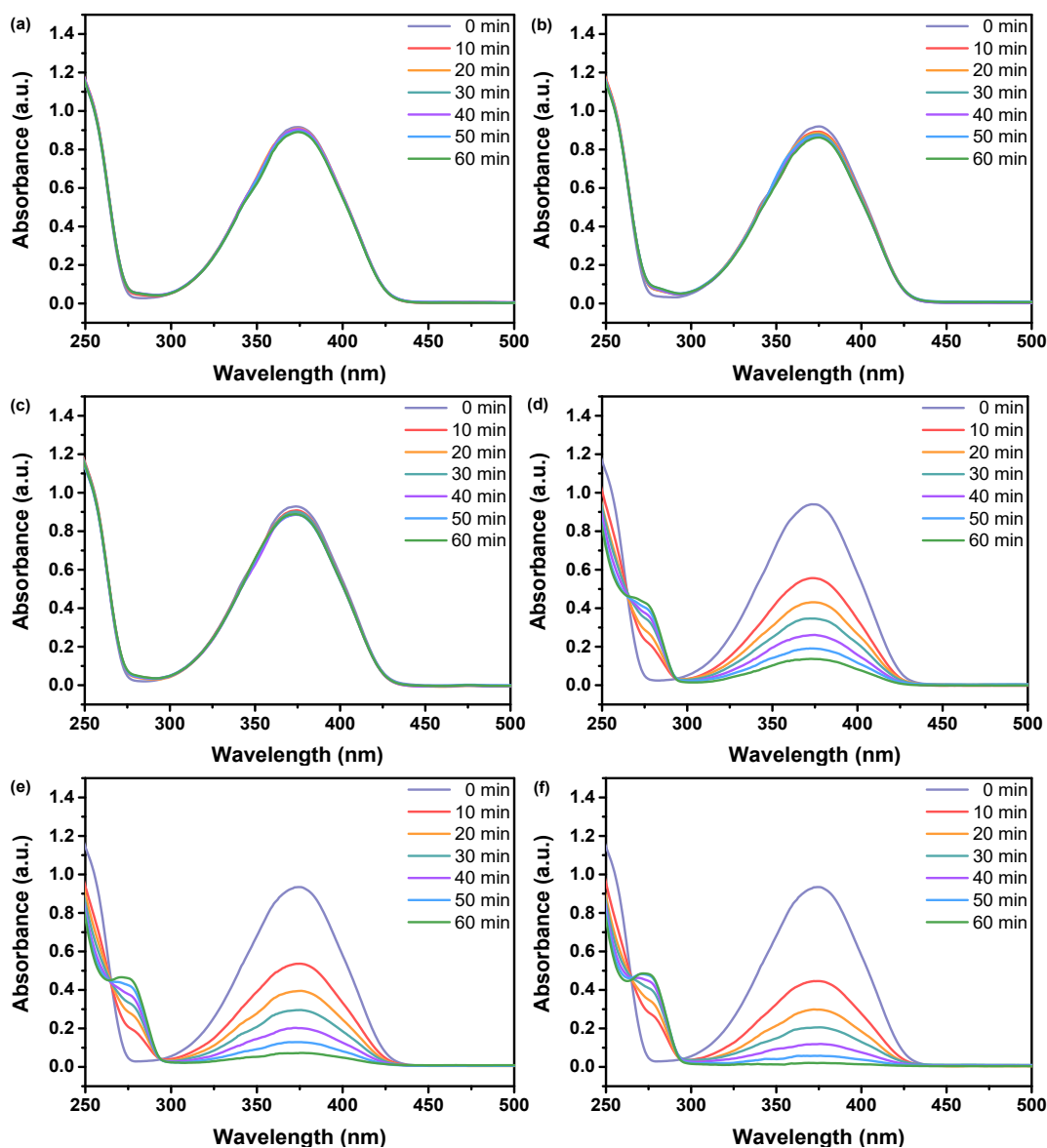


Figure S10. UV-vis absorption spectral change for the oxidation of 1,4-DHP (10^{-3} M) catalyzed by different catalysts under irradiation with a xenon lamp ($\lambda > 420$ nm). (a) $g\text{-C}_3\text{N}_4$; (b) CuTPP; (c) H_2TPP ; (d) CuTPP-Cy; (e) NiTPP-Cy; (f) H_2TPP -Cy.

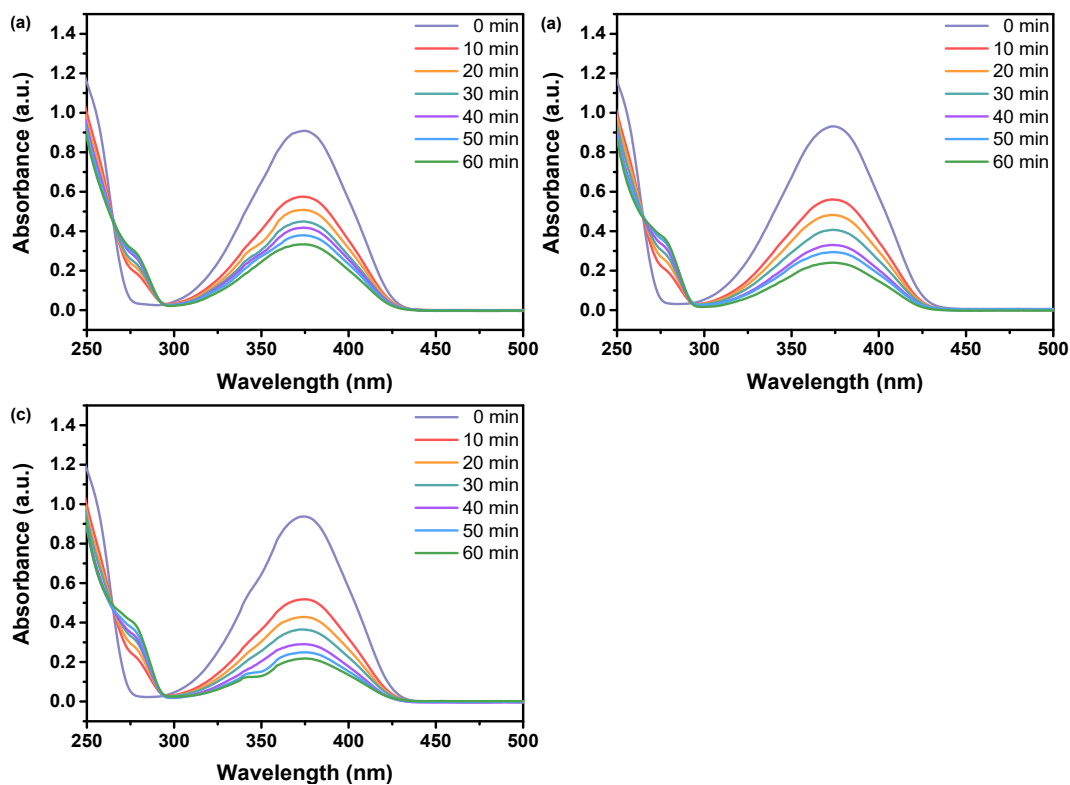


Figure S11. UV-vis absorption spectral change for the oxidation of 1,4-DHP (10^{-3} M) catalyzed by different catalysts in darkness. (a) CuTPP-Cy; (b) NiTPP-Cy; (c) H₂TPP-Cy.

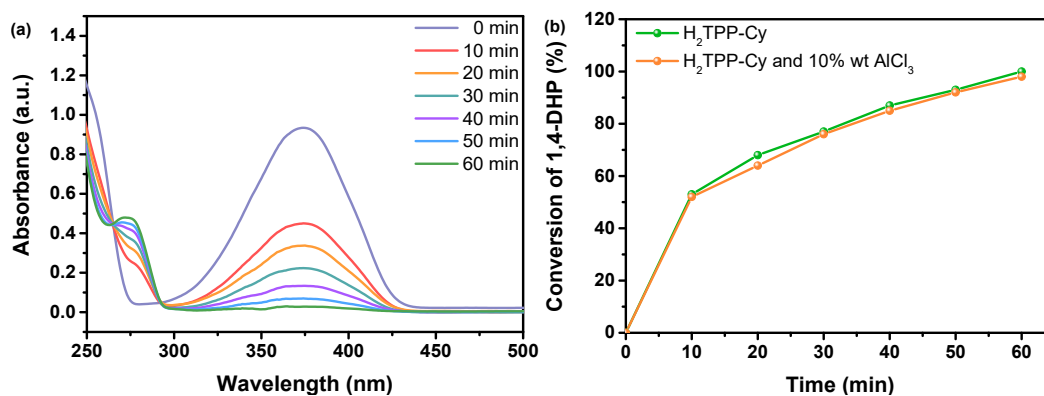


Figure S12. The oxidation of 1,4-DHP (10^{-3} M) catalyzed by H₂TPP-Cy and 10% wt AlCl₃ under irradiation with a xenon lamp ($\lambda > 420$ nm). (a) UV-vis absorption spectral change; (b) Comparison with H₂TPP-Cy.

7. ICP results of MTPP-Cys.

Table S2. ICP results of MTPP-Cys.

Catalysts	Al ³⁺ contents (wt%)	Ni ²⁺ contents (wt%)	Cu ²⁺ contents (wt%)
H ₂ TPP-Cy	0.226	0	0
NiTPP-Cy	0.120	0.361	0
CuTPP-Cy	0.652	0	0.834

8. Cycling stability of H₂TPP-Cy.

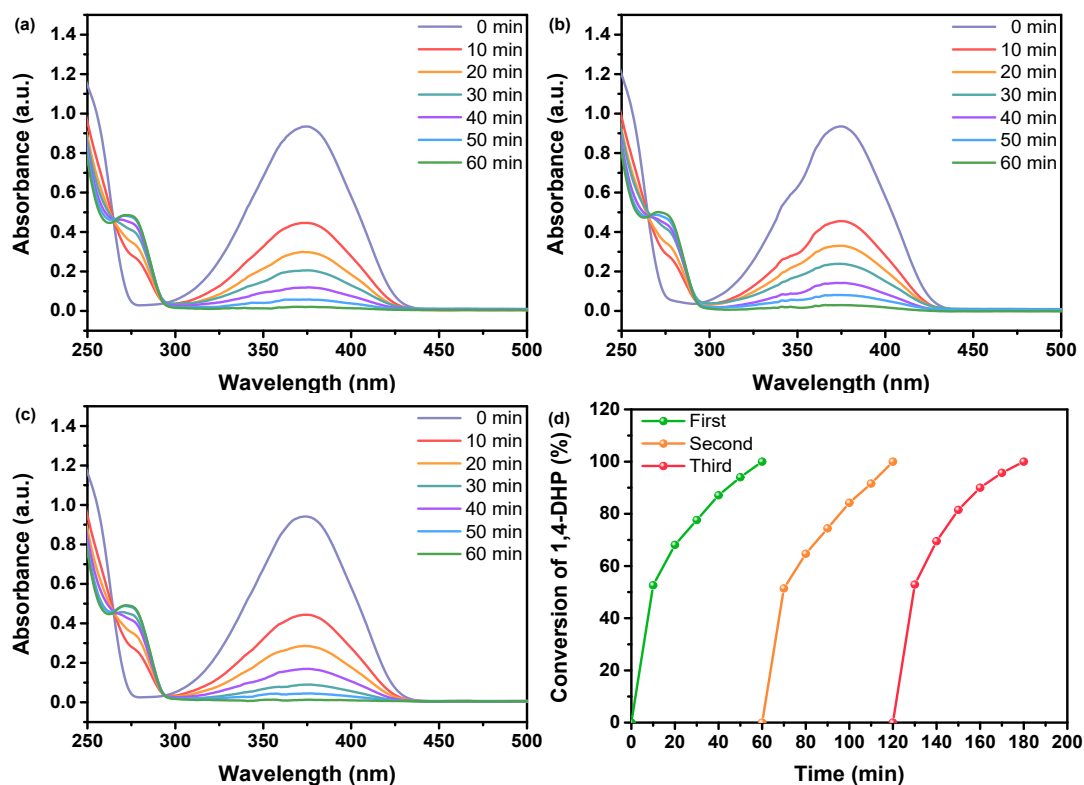


Figure S13. The durability of H₂TPP-Cy in photooxidation of 1,4-DHP (10⁻³ M) under irradiation with a xenon lamp ($\lambda > 420$ nm). (a) The first run; (b) The second run; (c) The third run; (d) The conversion of 1,4-DHP for three successive recycles.

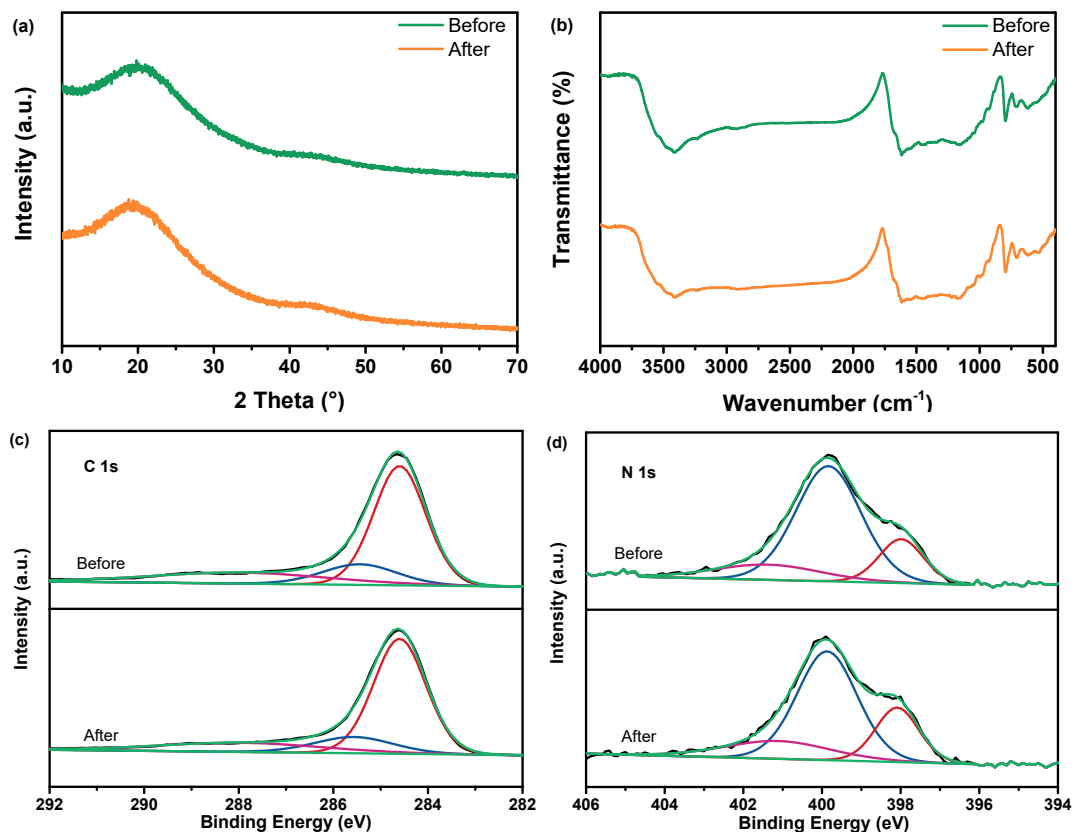


Figure S14. (a) XRD; (b) FT-IR; High-resolution (c) C 1s and (d) N 1s XPS spectra of H₂TPP-Cy before and after 3 times cycling experiments.

9. Summary of recently reported literatures for photooxidation of 1,4-DHP.

Table S3. Summary of oxidation of 1,4-DHP.

Catalyst	Conditions	$C_{1,4\text{-DHP}}/M$	Time/min	Con./%	Ref.
H ₂ TPP-Cy	darkness	10 ⁻⁴	≤20	>99	This work
	Xenon lamp (30 mW/cm ² , λ>420 nm).	10 ⁻⁴	≤10	>99	
	darkness	10 ⁻³	60	77	
	Xenon lamp (30 mW/cm ² , λ>420 nm).	10 ⁻³	≤60	>99	
C-120	Xenon lamp (60 mW/cm ² , λ> 385 nm)	10 ⁻⁴	≤30	>99	11
P-CN	Xenon lamp (100 mW/m ² , λ>385 nm)	10 ⁻⁴	≤40	>99	5
R-C ₃ N ₄	Xenon lamp (100 mW/m ² , λ> 420 nm)	10 ⁻⁴	≤40	>99	12
ZnCu-CDs-2	Xenon lamp (60 mW/cm ² , λ> 385 nm)	10 ⁻⁴	≤90	93.93	4
350-FeCu-CDs	xenon lamp (60 mW/cm ² , λ> 385 nm)	10 ⁻⁴	≤100	94.42	13
Cu-CDs-250	Xenon lamp (60 mW/cm ² , λ> 385 nm)	10 ⁻⁴	160	60.8	14

References

1. J. B. M. J. Tomasi, R. Cammi, Quantum Mechanical Continuum Solvation Models, *Chem. Rev.*, 2005, **105**, 2999-3093.
2. M. J. Frisch, *et al*, *Gaussian 09*, Gaussian Inc., Wallingford CT, 2009.
3. W. Wu, L. Zhan, W. Fan, J. Song, X. Li, Z. Li, R. Wang, J. Zhang, J. Zheng, M. Wu and H. Zeng, Cu-N dopants boost electron transfer and photooxidation reactions of carbon dots, *Angew. Chem. Int. Ed. Engl.*, 2015, **54**, 6540-6544.
4. W. Wu, Q. Zhang, R. Wang, Y. Zhao, Z. Li, H. Ning, Q. Zhao, G. P. Wiederrecht, J. Qiu and M. Wu, Synergies between Unsaturated Zn/Cu doping sites in carbon dots provide new pathways for photocatalytic oxidation, *ACS Catal.*, 2017, **8**, 747-753.
5. J. Zhang, X. An, N. Lin, W. Wu, L. Wang, Z. Li, R. Wang, Y. Wang, J. Liu and M. Wu, Engineering monomer structure of carbon nitride for the effective and mild photooxidation reaction, *Carbon*, 2016, **100**, 450-455.
6. J. Zhang, Y. Li, X. Zhao, L. Wang, H. Chen, S. Wang, X. Xu, L. Shi, L.-C. Zhang, Y. Zhu, H. Zhang, Y. Liu, G. Nealon, S. Zhang, M. Wu, S. Wang and H. Sun, Aligning potential differences within carbon nitride based photocatalysis for efficient solar energy harvesting, *Nano Energy*, 2021, **89**, 106357.
7. X. Wang, K. Maeda, A. Thomas, K. Takahashi, G. Xin, J. M. Carlsson, K. Domen and M. Antonietti, A metal-free polymeric photocatalyst for hydrogen production from water under visible light, *Nat Mater.*, 2009, **8**, 76-80.
8. Q. Q. Dang, Y. F. Zhan, X. M. Wang and X. M. Zhang, Heptazine-based porous framework for selective CO₂ sorption and organocatalytic performances, *ACS Appl. Mater. Interfaces*, 2015, **7**, 28452-28458.
9. J. Śniechowska, P. Paluch and M. J. Potrzebowski, Structure and dynamics processes in free-base chlorins controlled by chemical modifications of macroring and aryl groups in meso-positions, *RSC Adv.*, 2017, **7**, 24795-24805.
10. S. A. Vail, D. I. Schuster, D. M. Guldi, M. Isosomppi, N. Tkachenko, H. Lemmetyinen, A. Palkar, L. Echegoyen, X. Chen and J. Z. H. Zhang, Energy and electron transfer in β -alkynyl-linked porphyrin-[60]fullerene dyads, *J. Phys. Chem. B.*, 2006, **110**, 14155-14166.
11. X. Shao, W. Wu, R. Wang, J. Zhang, Z. Li, Y. Wang, J. Zheng, W. Xia and M. Wu, Engineering surface structure of petroleum-coke-derived carbon dots to enhance electron transfer for photooxidation, *J. Catal.*, 2016, **344**, 236-241.
12. W. Wu, J. Zhang, W. Fan, Z. Li, L. Wang, X. Li, Y. Wang, R. Wang, J. Zheng, M. Wu and H. Zeng, Remedying defects in carbon nitride to improve both photooxidation and H₂ generation efficiencies, *ACS Catal.*, 2016, **6**, 3365-3371.
13. Q. Zhang, W. Xu, C. Han, X. Wang, Y. Wang, Z. Li, W. Wu and M. Wu, Graphene structure boosts electron transfer of dual-metal doped carbon dots in photooxidation, *Carbon*, 2018, **126**, 128-134.
14. W. Wu, L. Zhan, W. Fan, J. Song, X. Li, Z. Li, R. Wang, J. Zhang, J. Zheng, M. Wu and H. Zeng, Cu-N dopants boost electron transfer and photooxidation reactions of carbon dots, *Angew Chem Int Ed Engl.*, 2015, **54**, 6540-6544.